CRYSTAL GROWTH & DESIGN

Subscriber access provided by - Access paid by the | UCSB Libraries

Anion-# interactions in hollow crystals of a copper(II)-cyamelurate coordination complex

Carla Martínez-Benito, Antonio Bauza, Ana B. Lago, Prof. Catalina Ruiz-Perez, Claudio A Jimenez, Manuel E. Torres, Antonio Frontera, and Jorge Pasán

Cryst. Growth Des., **Just Accepted Manuscript** • DOI: 10.1021/acs.cgd.8b00305 • Publication Date (Web): 07 Mar 2018

Downloaded from http://pubs.acs.org on March 7, 2018

Just Accepted

"Just Accepted" manuscripts have been peer-reviewed and accepted for publication. They are posted online prior to technical editing, formatting for publication and author proofing. The American Chemical Society provides "Just Accepted" as a service to the research community to expedite the dissemination of scientific material as soon as possible after acceptance. "Just Accepted" manuscripts appear in full in PDF format accompanied by an HTML abstract. "Just Accepted" manuscripts have been fully peer reviewed, but should not be considered the official version of record. They are citable by the Digital Object Identifier (DOI®). "Just Accepted" is an optional service offered to authors. Therefore, the "Just Accepted" Web site may not include all articles that will be published in the journal. After a manuscript is technically edited and formatted, it will be removed from the "Just Accepted" Web site and published as an ASAP article. Note that technical editing may introduce minor changes to the manuscript text and/or graphics which could affect content, and all legal disclaimers and ethical guidelines that apply to the journal pertain. ACS cannot be held responsible for errors or consequences arising from the use of information contained in these "Just Accepted" manuscripts.

ACS Publications

is published by the American Chemical Society. 1155 Sixteenth Street N.W., Washington, DC 20036

Published by American Chemical Society. Copyright © American Chemical Society. However, no copyright claim is made to original U.S. Government works, or works produced by employees of any Commonwealth realm Crown government in the course of their duties.

Anion-π interactions in hollow crystals of a copper(II)-cyamelurate coordination complex

Carla Martínez-Benito,[a] Antonio Bauzá,[b] Ana B. Lago,[a] Catalina Ruiz-Pérez,[a] Claudio A. Jiménez,[c] Manuel E. Torres,[d] Antonio Frontera,[b] and Jorge Pasán[a]*

[a] Laboratorio de Rayos X y Materiales Moleculares (MATMOL). Dpto de Física, Facultad de Ciencias (sección Fisica), Universidad de La Laguna (ULL). Avda. Astrofísico Francisco Sánchez s/n E-38204, La Laguna, Tenerife, Spain. E-mail: jpasang@ull.edu.es

[b] Departament de Química, Universitat de les Illes Balears, Ctra. Valldemossa km 7.5, E-07122 Palma de Mallorca, Illes Balears, Spain. E-mail: toni.frontera@uib.es.

[c] Departamento de Química Orgánica, Facultad de Ciencias Químicas, Universidad de Concepción, Casilla 160-C, Concepción. Chile. E-mail: cjimenez@udec.cl.

[d] Departamento de Física, Facultad de Ciencias (Sección Física), Universidad de La Laguna (ULL). Avda. Astrofísico Francisco Sánchez s/n E-38204, La Laguna, Tenerife, Spain.

KEYWORDS. Crystal morphology, hollow structure, anion···π interaction, heptazines, coordination compounds

0. Abstract

A novel cyamelurate-based copper(II) coordination compound has been designed from a computational approach to show anion-π interactions between the s-heptazine core and perchlorate anions, therefore a complex of formula $\{[Cu(pmta)]_3cyam\}(ClO_4)_3$ (**1**) [pmta = *N*,*N*,*N*',*N*'',*N*''-pentamethyl-diethylenetriamine and cyam = cyamelurate ligand] was synthesized. The cationic molecule stabilizes in the solid state with two perchlorate anions one above and the other below the cyamelurate aromatic rings in a polar conformation, crystallizing in the *R*3*c* non-centrosymmetric space group with a close cubic packing of the cations. The binding energies were calculated to be *ca.* –175 kcal/mol for the two species **1**:$OClO_3^-$ and **1**:O_3ClO^-, and the anion-π contribution could also be calculated, being *ca.* –10 kcal/mol. The dielectric and magnetic properties were analyzed showing a semiconductor behavior in the temperature range studied (300 – 458 K) and a weak antiferromagnetic interaction among the three Cu(II) ions. The crystals of **1** show a hollowed hexagonal prismatic morphology, with hollow diameters up to 300 microns. A mechanism based on oriented growth, dissolution and recrystallization of the outer shell was proposed to explain these hollowed structures.

1. Introduction

Supramolecular chemistry of anions is an area of incessant interest due to key role of that anions play in many important chemical and biological processes.[1,2] The anion–*π* interaction is gaining interest, not only because it is a well recognised interaction that plays important roles in biological functions,[3] but also for constructing anion binding receptors, and a new family based on this interaction is emerging in the literature, and numerous examples have been reported so far.[4-7] Theoretical studies have demonstrated that the strength of the anion–π interaction depends upon the magnitude of the quadrupole moment and the molecular polarizability.[8] Therefore a convenient aromatic ligand should have an extended π-system (high polarisability) and be electron deficient (high positive quadrupole moment).

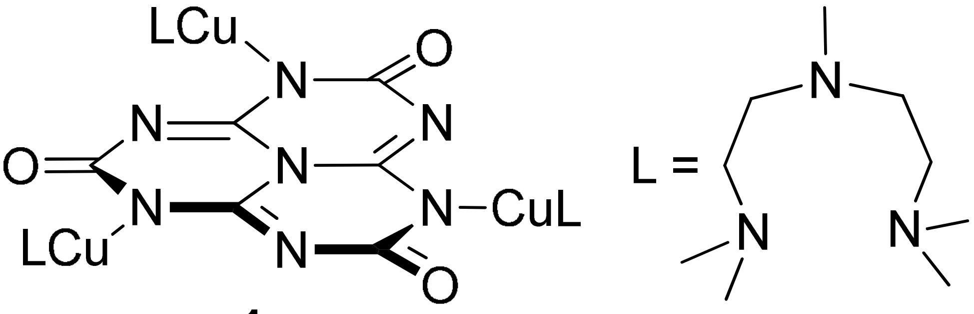

1

Scheme 1

The cyameluric acid (Scheme 1), a molecule part of the *s*-heptazine family, satisfies both requirements (three electron deficient fused rings) and, additionally, it has been previously proposed theoretically as a novel anion-π binding block for building tripodal receptors.[9] This previous knowledge recognizes this molecule as the ideal candidate to design a strong anion binding system but, up to now, anion-π interactions have not been reported experimentally in any of the *s*-heptazine systems. The use of metal centers to coordinate electron deficient aromatic systems strongly affects the *π*-acidity of the ligand, thus increasing the strength of the anion–*π* interaction.[10] Indeed, triazine based copper(II) complexes have been explored in the search of these interactions.[11] The coordination chemistry of the cyamelurate ligand has been scarcely explored and only a few complexes have been reported.[12-15] Among them, only tin(II)-cyamelurate complex exhibits an interaction between a solvent dichloroethane molecule and the heptazine, with a Cl···N distance of 3.47 Å.[13] With this knowledge in mind, we have designed and synthetized a novel trinuclear copper(II) complex with the cyamelurate ligand of formula

$\{[Cu(pmta)]_3cyam\}(ClO_4)_3$ (**1**) [pmta = *N*,*N*,*N*',*N*",*N*"-pentamethyl-diethylenetriamine and cyam = cyamelurate ligand], where interactions among the perchlorate anions and the heptazine core are envisaged by theoretical calculations.

The crystal growth of hollow structures is an intriguing phenomenon, although formation of hollow crystals have been extensively reported for metals,[16] inorganic salts,[17] complexes[18] and organic compounds.[19-22] The commonplace for all these structures is the anisotropy of the crystallization which leads to tubular structures where growth mechanisms have been proposed such as the perpetuation in one-dimension of screw dislocations of large magnitude.[17] Other structures, like octahedra or microspheres can be constructed hierarchically with the aid of templates,[23,24] and a case has been reported of a single crystalline hollow icositetrahedron obtained from a one-pot hydrothermal synthesis with a reversed crystal growth mechanism.[25] In general, tubular crystals with micrometer hollow diameters are still rare, Pérez-Hernández *et al.* and Castillo-Blas *et al.* have reported tubular crystals with hollow diameters of hundreds of microns,[26,27] but even so, the hollow plate crystals of **1** represents an oddity. Mechanisms to explain the apparition of hollow structures includes the abovementioned screw dislocation system, or an Ostwald ripening process where the outer shell of the crystal grows at the cost of the smaller core crystals.[18,19,26-28]

In this work, based on a computational approach, we have designed and synthesized a new material intended to show strong anion-π interactions between the perchlorate anions and the heptazine core. We have calculated the binding energies of the anion-π interaction, separating the electrostatic and H-bond contributions. We have also studied the dielectric and magnetic properties of the $\{[Cu(pmta)]_3cyam\}(ClO_4)_3$ (**1**) complex and particularly, the hollow hexagonal prismatic habit in which they crystallize.

2. EXPERIMENTAL SECTION

2.1. Materials and methods

The reagents copper(II) perchlorate hexahydrate, *N*,*N*,*N*',*N*",*N*"-pentamethyl-diethylenetriamine (pmta) and ethanol, were purchased from Sigma-Aldrich and used without further purification. Potassium cyamelurate was synthetized according to a reported procedure[13] with small modifications (see SI). The microscopic morphology of the material was examined by a JSM6300 scanning electron microscope (JEOL, Tokyo, Japan) and a Nikkon SMZ1000 Stereoscopic Microscope equipped with a Sony Color Digital camera DFW-SX910/X710.

2.2. Physical measurements

IR spectra (450-4000 cm^{-1}) were recorded on a powder sample by means of Shimadzu IRAffinity1 spectrophotometer equipped with a Pike technologies GladiATR. Thermogravimetric analysis on freshly crushed crystals of **1** was carried out in a Perkin-Elmer Pyris Diamond TG/DTA thermal analyzer, typically using a few mg samples placed on an alumina crucible under a nitrogen atmosphere at a flow rate of 20 cm^3 min^{-1}. The temperature was ramped from 25 to 250 ºC and at a heating rate of 5 ºC min^{-1}. Dielectric measurements were carried out on a non-hollowed crystal of **1** with size of 3 x 3 mm and thickness of 0.86 mm, using a Hewlett-Packard 4192A impedance analyzer which was controlled by a computer. The electric field was applied along the *c* crystallographic axis of the sample, being both hexagonal surfaces of the sample coated with silver paste to make contact between the crystal and the cell electrode.[29] Then crystal was placed in the cell (parallel plate capacitor)[30] and measurements were recorded during a heating and cooling cycle, in the frequency range of $10^3 – 10^6$ Hz with an applied voltage of 1 V, over the temperature range of 310 to 460 K dynamically scanned with a rate of 0.7 K min^{-1}. Magnetic susceptibility measurements on crushed crystals of **1** were carried out in the temperature range 2-300 K with a Quantum Design SQUID magnetometer under applied dc magnetic fields of 5000 Oe (2 K $< T <$ 30 K) and 10000 Oe (30 K $< T <$ 300 K). Corrections for the diamagnetic contribution of the constituent atoms were applied. The magnetic data were also corrected for the temperature-independent paramagnetism [60 cm^3 mol^{-1} per Cu(II)] as well as for the magnetization of the sample holder.

2.3. Computational details

All calculations were carried out using the turbomole package version 6.4[31] using the BP86-D3 method, which has been used to study noncovalent interactions using the crystallographic coordinates optimizing the entire X-ray geometry. In this study, def2-TZVP basis set was used. For the calculations we have used the BP86 functional with the latest available correction for dispersion (D3).[32] The *ab initio* calculations of the H_3cyam:$OClO_3^-$ and H_3cyam:O_3ClO^- complexes were performed at the RI-MP2/def2TZVP level of theory. The interaction energies were calculated with correction for the basis set superposition error (BSSE) by using the Boys-Bernardi counterpoise technique.[33]

2.4. Synthetic Procedure

The synthesis of the complex **1** was carried out by slow evaporation at room temperature. The preparation detailed here is that optimized to give the best yield.

Warning. Perchlorate salts containing organic ligands are potentially explosive. We work in solution at the mmol scale and the products were obtained by slow evaporation of the mother solutions in a hood at room temperature.

{[Cu(pmta)]$_3$cyam}(ClO$_4$)$_3$ (1). The $[Cu(pmta)]^{2+}$ precursor was prepared by the reaction of copper(II) perchlorate hexahydrate (278 mg, 0.75 mmol) with *N*,*N*,*N*',*N*'',*N*''-pentamethyldiethylenetriamine (0.156 cm^3, 0.75 mmol) in a water/EtOH 50/50 solution (10 cm^3). The dark blue solution of [Cu(pmta)]$^{2+}$ was dropwise added to another water/EtOH 50/50 solution (10 cm^3) of potassium cyamelurate and the final solution was stored at room temperature and allowed to slowly evaporate. After a few days, deep blue hexagonal prisms of **1** were grown. They were filtered, washed with ethanol and air dried. Yield: 72% (based on Cu). IR (cm^{-1}): 1552s, 1465m, 1406s, 1394s, 1166m, 1082vs, 1041s, 1012m, 960m, 939m, 925m, 804s, 773m, 621s.

2.5. X-ray crystallographic data collection and structure solution

X-ray crystallographic data for **1** were collected at 100 K in the ESRF synchrotron facilities at the BM16 beamline (Grenoble, France) with λ = 0.738 Å. Data were indexed, integrated and scaled with the HKL2000 software.[34] The crystal structure was solved by direct methods and refined with the full-matrix least squares techniques of F^2 by using SHELXS and SHLEXL programs[35] included in the WINGX software package.[36] All non-hydrogen atoms were refined anisotropically. The hydrogen atoms of the organic ligands were set on geometrical positions and refined with a riding model. The final geometrical calculations and the graphical manipulations were carried out with the PLATON[37] and DIAMOND[38] programs. A summary of the crystal data and refinement details is listed in Table 1, whereas selected bond lengths and angles are shown in Table S1. Crystallographic data have been deposited at the Cambridge Crystallographic Data Centre with CCDC reference number 977070.

Table 1. Crystallographic Data for **1**.

Compound	**1**
Formula	$C_{33}H_{69}N_{16}O_{15}Cu_3Cl_3$
FW	1227.01
Crystal System	Trigonal
Space group	*R*3*c*
a, Å	13.372(2)
b, Å	13.372(2)

c, Å	48.815(10)
V, Å^3	7559(3)
Z	6
Index ranges	$-18 \leq h \leq 17$ $-17 \leq k \leq 18$ $-63 \leq l \leq 63$
T, K	100(2)
ρ_{calc}, Mg m^{-3}	1.617
λ, Å	0.738
μ, mm^{-1}	1.651
Total reflections	46408
Indep. reflections (R_{int})	4572 (0.0503)
Flack parameter	0.002(11)
R_1, $I>2\sigma(I)$ (all data)	0.0270 (0.0278)
wR_2, $I>2\sigma(I)$ (all data)	0.0658 (0.0666)
Goodness-of-fit	1.068

3. RESULTS AND DISCUSSION

3.1. Description of structure of $\{[Cu(pmta)]_3cyam\}(ClO_4)_3$ (1). The compound crystallizes in the non-centrosymmetric trigonal $R3c$ space group and its crystal structure consist of cationic trinuclear entities of formula $\{[Cu(pmta)]_3cyam\}^{3+}$ and perchlorate anions (Figure 1). The trinuclear units are formed by a central cyam^{3-} group acting as a tritopic ligand towards three copper(II) ions whose coordination environments were partially blocked by the chelating pmta molecules. In the asymmetric unit there are one copper(II) ion, one pmta molecule, one third of the cyam ligand and three thirds of perchlorate ions. The rest of the molecule is symmetry generated by a three fold axis that crosses through the central cyamelurate nitrogen atom [N(2)]. The cyam ligand is linked to the copper atom through a nitrogen atom [N(1)] and an oxygen atom [O(1)] (Table S1).

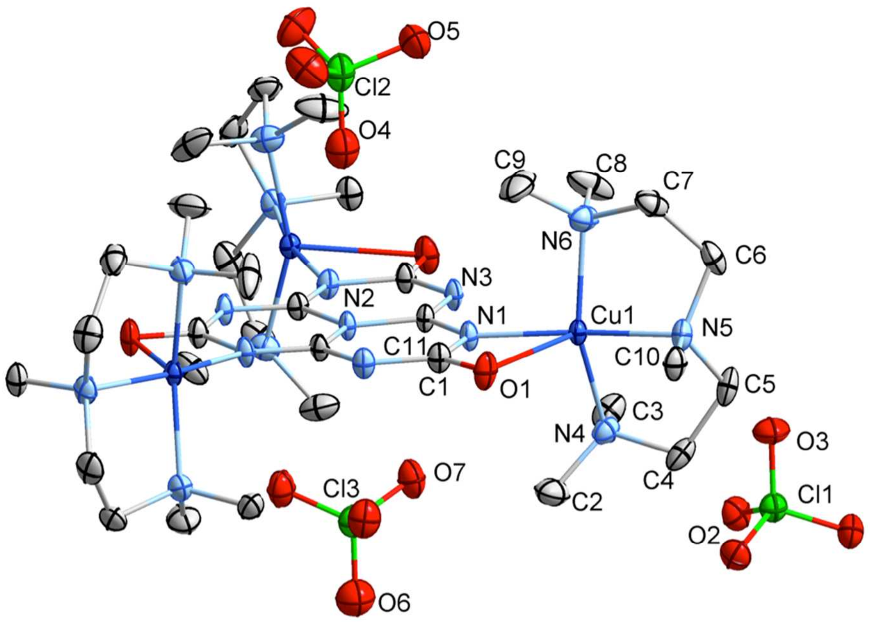

Figure 1. A view of the structure of **1** showing the anion-π system and the three crystallographically independent perchlorate anions. The numbering scheme has been added only for atoms in the ASU unit. The ellipsoids represent 50% probability. Hydrogen atoms have been omitted for clarity.

The copper(II) ion is four-coordinate with a distorted square planar environment [the value of the distortion parameter τ_4 is 0.256, τ_4 being 1 for a perfect tetrahedral geometry and 0 for a perfect square planar geometry].[39] The CuN_4 chromophore is formed by four nitrogen atoms, three from the pmta [N(4), N(5) and N(6)] and one from the cyamelurate [N(1)], being the average bond length 2.019(3) Å. There is a long Cu–O interaction with the oxygen atom of the cyamelurate [Cu(1)–O(1) bond distance being 2.480(3) Å] leading to a very distorted square pyramidal environment around the Cu(1). The angle between the Cu(1)–O(1) bond and the normal of the CuN_4 basal plane is 27.05(6)º.

Each $\{[Cu(pmta)]_3cyam\}^{3+}$ molecule is connected to other six through weak C–H···O hydrogen bonds in the *ab* plane (Figure 2). In the *c* direction there is a regular alternate stacking of one layer of perchlorates and one layer of $\{[Cu(pmta)]_3cyam\}^{3+}$ molecules (Figure 3). Considering only the cationic molecules, they are arranged in a cubic close packing of *ABCABC* sequence, a situation not uncommon for bulky cations and small anions.[40,41] Both, the cations and the perchlorate molecules are located on the three-fold symmetry axes (6a Wyckoff site) (Figure S1), however, the ClO_4^- anions occupy the three 6a positions within each layer, but the bulky cations occupy only one of them in each layer. This results in a polar arrangement of the perchlorate anions (Figure 3). Two perchlorate anions are located above and below the cyamelurate ring establishing anion-π interactions in a $OClO_3$···cyam···$OClO_3$ polar arrangement [N(2)···O(7) is 3.465(4) Å for the $OClO_3$···cyam interaction and N(2)···O(4) is 3.327(7) Å for the cyam···$OClO_3$ interaction].

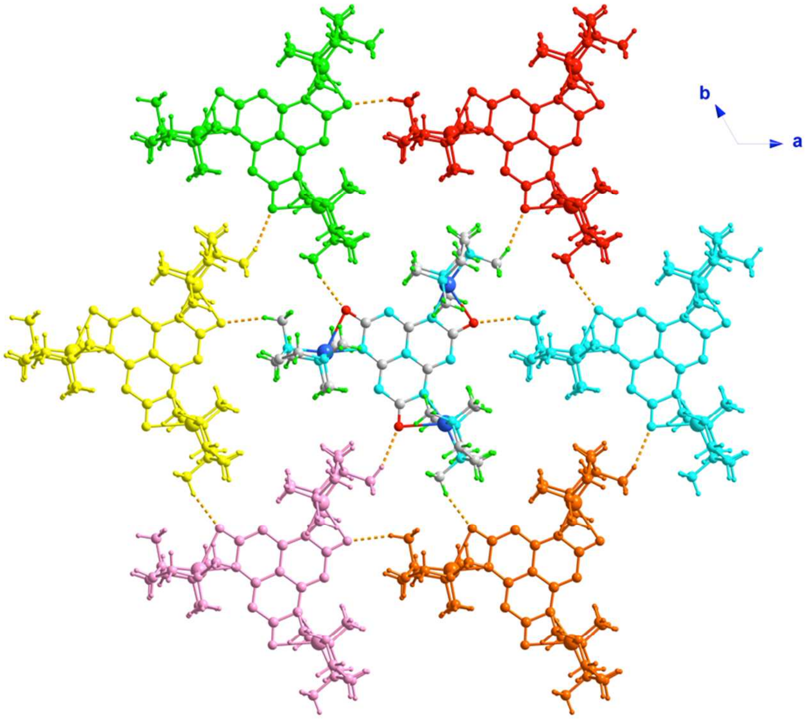

Figure 2. Crystal packing of the cations of **1** in the *ab* plane, showing the C–H···O weak interactions between the trinuclear molecules (dashed orange lines).

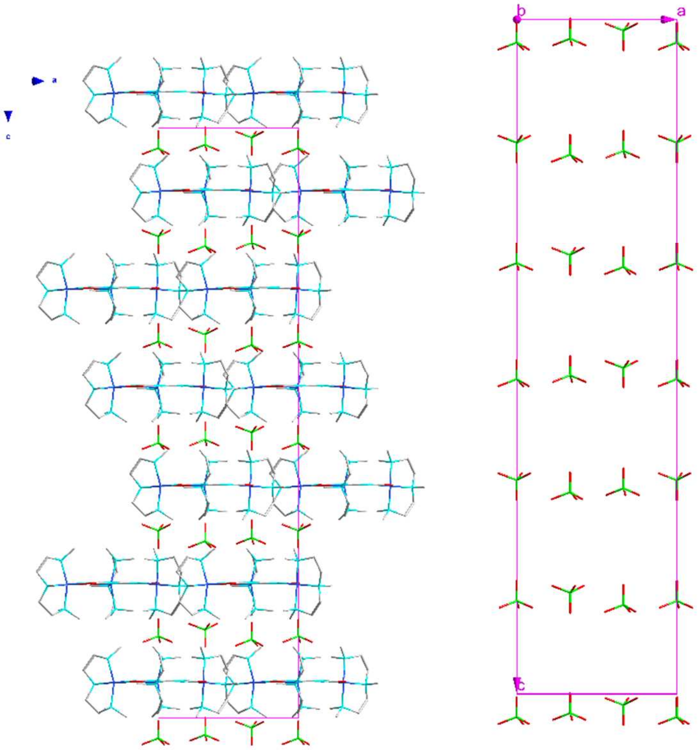

Figure 3. Projection along the crystallographic *b* axis of the crystal structure of **1**, showing one unit cell (left) and a detail of the polar arrangement of the perchlorate anions in the unit cell (right).

3.2. Anion-π interaction

Theoretical studies have demonstrated that the strength of the anion–π interaction depends upon the magnitude of the quadrupole moment and the molecular polarizability.[5,8,42] The molecular electrostatic potential (MEP) surface for the cyamelurate ligand (see Figure 4) shows an extended region above and below the aromatic system with positive (blue color) electrostatic potential, susceptible to interact with anions. This model system has been computed using *ab* *initio* and DFT calculations (see above for computational details). Starting by computing a simple 1:1 complex between cyameluric acid (**H$_3$cyam**) and perchlorate anion at both high level *ab initio* (RI-MP2) and DFT (BP86-D3) in order to validate the DFT method. As can be observed from the results gathered in Table 2, both methods give almost identical results.

Table 2. Interaction energies with BSSE correction (ΔE, kcal/mol) and equilibrium distances (d, Å) for several complexes of **cyam** and **1** with ClO_4^-

Complex	**ΔE**	**d**[a]
H$_3$cyam:$OClO_3^-$	–21.6 (–21.8)[b]	2.525
H$_3$cyam:O_3ClO^-	–27.6 (–27.2)[b]	2.754
1:$OClO_3^-$	–174.4	2.698
1:O_3ClO^-	–174.5	2.825
1*:$OClO_3^-$	–20.0	2.698
1*:O_3ClO^-	–16.0	2.825
1*L*:$OClO_3^-$	–13.6	2.698
1*L*:O_3ClO^-	–7.3	2.825

[a] Measured from the closest O atom of the anion to the ring mean plane.
[b] Values in parenthesis correspond to RI-MP2/def2-TZVP level of theory.

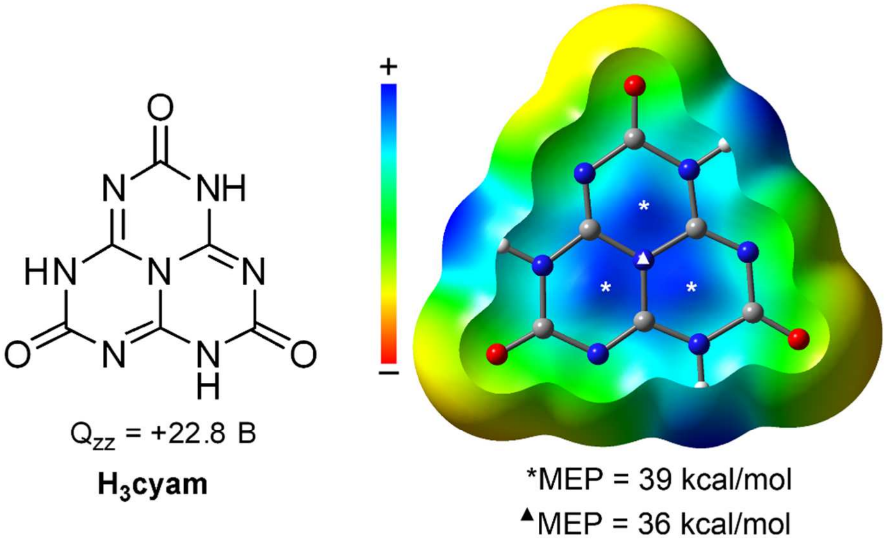

Figure 4. Left: Quadrupole moment (Qzz) of cyameluric acid. Right: representation of the molecular electrostatic potential (MEP) surface of cyameluric acid.

The optimized complexes denoted as **1**:$OClO_3^-$ and **1**:O_3ClO^- (indicating one or three oxygen atoms, respectively, pointing to the cyameluric π-system) are represented in Figure S2. In both complexes (**1**:$OClO_3^-$ and **1**:O_3ClO^-), very short anion–π distances and a large number of hydrogen bonds that fix the orientation of the anion over the ring are observed. The C–H···O hydrogen bonds are energetically favoured by the coordination the **L** ligand to the Cu(II) atom that increases the acidity of the hydrogen atoms of the methyl groups. It is worth mentioning the perfect fitting between the chloride anion and the receptor and that the position of the oxygen atoms of the anion is close to the location of the MEP minima of the cyam moiety (see Figure 4). Clearly the final position is a compromise between preferred conformation dictated by the MEP (maximizing the anion–π interaction strength) and the hydrogen bonding network governed by the C–H···O interactions.[43]

Additional complexes have been computed in order to know the relative importance of the different contributions to the total interaction energy and results are included in Table 2. The binding energies of the complexes between **1** and perchlorate (**1**:$OClO_3^−$ and **1**:$O_3ClO^−$) are very large and negative (-174 kcal/mol) indicating a strong interaction, which is basically due to the electrostatic attraction between the host (net charge +3) and the anion. To estimate the contribution of the pure electrostatic effects we have computed the interaction energies using Cu(I) instead of Cu(II), and consequently the host becomes neutral (denoted as **1***). By doing so the interaction energies are drastically reduced to –20.0 and -16.0 kcal/mol for **1***:$OClO_3^−$ and **1***:$O_3ClO^−$, respectively, indicating that the simple electrostatic attraction between the counterparts is the main force. However, the anion–π and H-bonding interactions are also important and certainly contribute to the final position of the perchlorate, since both interactions are directional. Finally, we have computed the interaction energies replacing the methyl groups of the triamine ligand by hydrogen atoms (denoted as **L***). The interaction energies are further reduced to –13.6 and –7.3 kcal/mol (for **1*L***:$OClO_3^−$ and **1*L***:$O_3ClO^−$, respectively), which can be attributed to the anion–π interaction. These interaction energies are comparable to those previously computed in neutral aromatic rings.[5,8,42]

The space group of the crystal structure is *R*3*c*, in sharp agreement with the C_3 symmetry found for the **1**:$OClO_3^-$ and **1**:O_3ClO^- binary complexes. In addition, the solid state structure shows that the anion-π system is able to incorporate two anions at opposite sides of the heptazine ring, each one using a different orientation (one or three oxygen atoms pointing to the π-system). This also agrees with the energetic results of Table 2 that shows that both complexes are almost isoenergetic (~174 kcal/mol). This situation causes the crystal structure to be non-centrosymmetric with a polar arrangement of the perchlorate anions within the structure (see Figure S2).

The first polyatomic anion is embraced by the π-acidic cavity with CH···O interactions and a short distance O···$N_{heptazine}$ of 3.327 Å, the second perchlorate anion have three O···heptazine centroid distances of 3.290 Å (see Figure S3). Both distances are in agreement with the latest proposed anion-π criterion, where the anion to carbon(nitrogen) atom distances ≤ sum of van der Walls radii (ΣR_{vdW}) + 0.8 Å.[44] Since the system is able to establish two simultaneous anion–π interactions forming ternary complexes, those have been also optimized using DFT calculations. As a result, very favourable interaction energy (-297 kcal/mol) have been obtained, however it is considerably lesser (in absolute value) than the sum of the interaction energies obtained for the binary complexes **1**:$OClO_3^-$ and **1**:O_3ClO^- (see Table 2), as a consequence of the electrostatic repulsion of two anions located at opposite sides of the cyamelurate molecular plane. These ternary anion–π–anion complexes have been previously described in the literature by Domasevitch et al.[45] in pyridazino[4,5-d]pyridazine coordinated to silver(I).

3.3. Dielectric Properties

Dielectric properties of **1** were studied by measuring the complex impedance $Z^*(\nu)$. In the 313 < T < 433 K temperature range the values of ε_r' are practically constant with a value at 433 K of 7.2 for 5.6 kHz and 5.0 for 1 MHz. Upon heating, ε_r' smoothly increases until 453 K (ε_r' being 222 for 5.6 kHz and 23.5 for 1 MHz), to finally show an abrupt growth to reach 458 K (ε_r' being 6280 for 5.6 kHz and 101.0 for 1 MHz), see Figure 5. The values of ε_r' decrease when the frequency is increased, from 13.3 (5.6 kHz) to 5.41 (1 MHz) at 313K and from 6280 (5.6 kHz) to 101.0 (1 MHz) at the highest temperature reached. This decrease of ε_r' with the increasing frequency can be explained as follows: At low frequencies, there is a contribution to ε_r' of the four polarization mechanisms (electronic, ionic, orientation and space charge), but as the frequency increases, the dipoles cannot follow the applied field and the contribution of the orientation polarization decreases, and therefore ε_r' does, approaching a practically constant value for each temperature at higher frequencies (see Figure S4).[46]

The analysis of the conductivity spectra was based on the universal dielectric response,[46] an empirical power law that can be expressed as:

$$\sigma'(\upsilon) = \sigma_{dc} + A\upsilon^s = \sigma_{dc}\left[1 + \left(\frac{\upsilon}{\upsilon_p}\right)^s\right] \quad (1)$$

where σ_{dc} is the direct current conductivity for a particular temperature, ν_p is the crossover frequency, s is a fractional exponent with values between 0 and 1 depending on many-body interactions among charge carriers and their surroundings [being 1 (Debye behaviour), a negligible interaction and $s < 1$, stronger interactions],[47] and A is a temperature-dependent preexponential factor which is related to the polarisability.[48] In this model, each conduction mechanism leads to different frequency and temperature dependences for the conductivity (σ') and the *s* exponent. Fits to this equation can be found in the Supplementary Information (Figure S5).

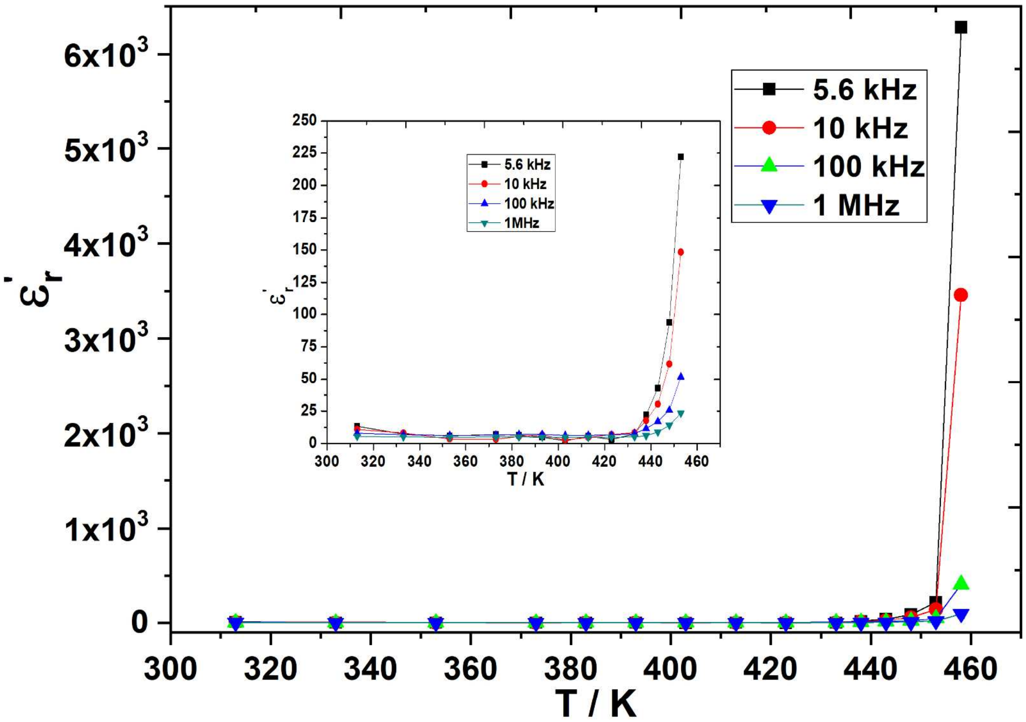

Figure 5. Real part of the complex permittivity as a function of the temperature at different frequencies (5.6 kHz, 10 kHz, 100 kHz and 1 MHz) for **1**. The inset shows the temperature dependence of ε_r' in the range between 313 and 453 K.

In the range of temperatures explored and due to the increase of σ_{dc} with the temperature, this material exhibits a semiconductor behavior.[49] The *s* parameter grows smoothly with the temperature until *ca.* 383 K, and then it decreases to reach a minimum at 453 K (see Figure S6).

This situation is associated with a greater interaction of the charge carriers with its surroundings.[47] Regarding the behaviour of the *A* parameter, the *s* trend is reversed, reaching its higher value, and therefore, the greater polarizability of the system, at 453 K, where *s* is minimum (Table S2). These two different behaviours can be related with the change on the perchlorate anion environments which affect the mobility of the charge carriers.

The conductivity of the crystal (σ') presents an increment near of two orders of magnitude between 453 and 458 K, Figure S5. At 458 K, $\square_r'$ and σ' not only reach their higher values, but these are much larger than those observed at lower temperatures (See Figures 5 and S5). The activation energy for the process occurring at *ca.* 458 K can be derived from the slope of σ_{dc} (Figure S7), giving a value of 348 kcal/mol. This value is obtained using only two points due to the impossibility of going over 480 K without degradation of the material, but it turns out to be comparable to the total value of the energy calculated for the anion-π interaction of $OClO_3^-$:**1**:$OClO_3^-$ (297 kcal/mol). In the crystal structure, along the *c* axis, each row of molecules is formed by the periodic arrangement of three perchlorate anions (up – down - up) and a $[Cu(pmta)_3cyam]^{3+}$ group in a polar ···*UDU(cyam)UDU(cyam)*··· sequence (Figure 3). This could suggest that the loosen of the anion-π interactions lets the perchlorate anions to show a better disposition to favour the polarization, for example a complete polar situation of three ups or three downs. The broad exothermic pick between 300 and 470 K without loss of mass, which could be also associated with a re-organization of the perchlorates, in the TG-DTA experiment can also support this explanation (Figure S8).

3.4. Magnetic properties

The magnetic properties of **1** are presented in the form of $\chi_M T$ vs. T [χ_M being the magnetic susceptibility per three copper(II) ions] plot (Figure S9). At room temperature the value of $\chi_M T$ is

1.197 $cm^3 mol^{-1}$ K, as expected for three magnetically isolated spin doublets. Upon cooling, this value remains constant and only at very low temperatures starts to decrease to reach 1.146 $cm^3 mol^{-1}$ K at 2 K. The magnetic data follows a Curie Law, and only at very low temperatures some antiferromagnetic interactions are encountered. We, therefore, analysed the data with a Curie-Weiss expression introducing a theta parameter to take that antiferromagnetic interactions into account. The best-fit curve matches the experimental data in the whole temperature range, being the values of $g = 2.057(1)$ and $\theta = -0.050(3)$ K. The main magnetic exchange pathway among the copper(II) ions in **1** is the heptazine ligand, which, although being an electron delocalized platform is electron deficient and therefore, poor overlap of the magnetic orbitals is expected.

3.5. Crystal morphology

The habit of the crystals of **1** deserves a separate section. The crystals obtained following the experimental procedure described above are blue hexagonal prisms, which in a closer look, have a depression in the center (Figure 6, left). This depression grows to finally obtain hollowed crystals (Figure 6, rigth).

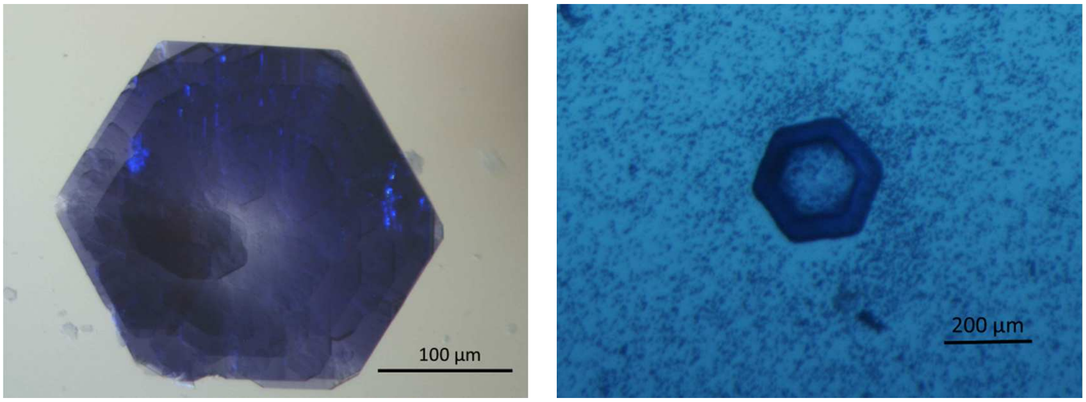

Figure 6. Left: Crystal of **1** with a lower crystal density in the core. Right: Crystal of *ca.* 300 µm with a well-defined hexagonal void of approx. 250 µm diameter in the center.

SEM images of these crystals show that they are composed of sheet-like crystals stacked along the hexagonal axis, whereas in the hollow central section few broken crystals are observed (Figure 7a). In other cases intertwinned crystals with a central depression are observed (Figures 7b and 7c), and even crystals with a depression and a hollow core (Figure 7d).

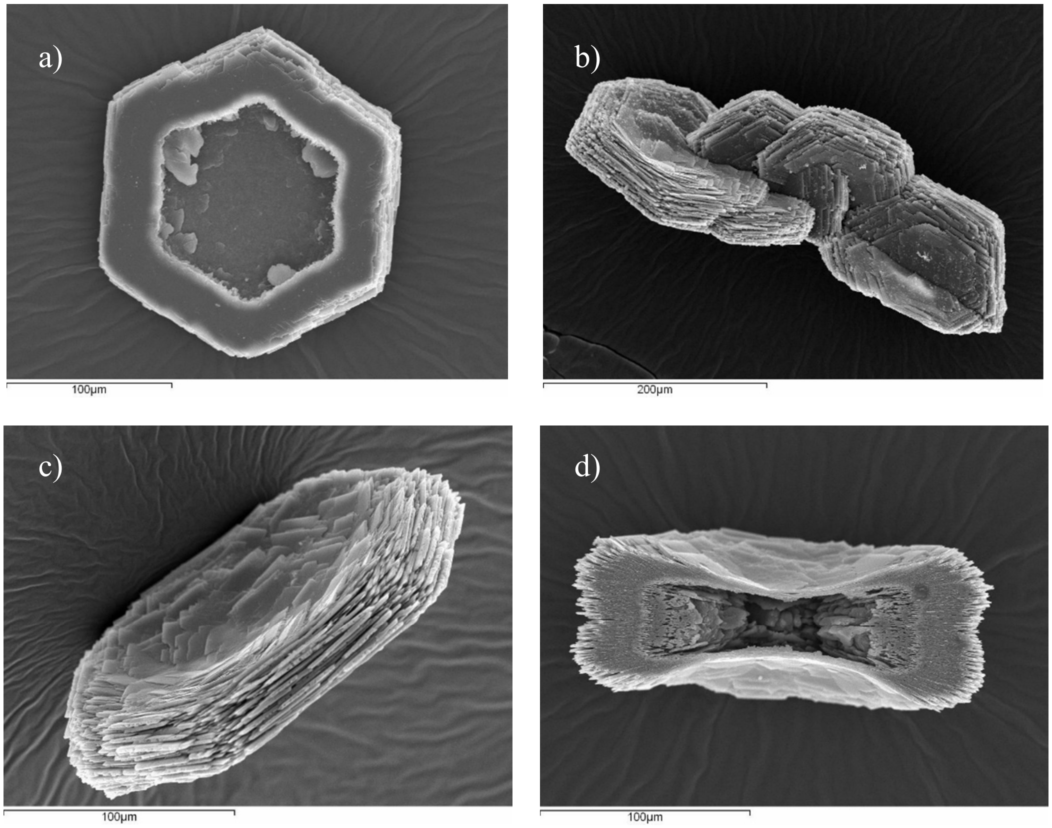

Figure 7. SEM images of the crystals of **1** showing a) the hollowed crystal with hexagonal prism morphology; b) intertwinned crystals; c) a side view of a hexagonal crystal with a depression at the core, and d) a side view of a crystal with a depression showing the hollow interior.

However, in the X-ray diffraction experiment, although a twin was measured, there was a main component responsible for most of the reflections, suggesting that if the crystal is constituted of several sheet-like crystals, they most likely have the same relative orientation. The hexagonal prisms have a very small height, they very slowly grow in the (001) direction, and the rectangular faces correspond to the (110), (-120) and (2-10) planes (Figure 8). At some point during the crystal growth, the crystal presents a dodecagonal prism habit being the (100), (010) and (1-10) faces those that disappear (Figure 8 and S10). Indeed, the vertices of the hexagon are sometimes truncated to form a truncated hexagonal prism (Figure 9).

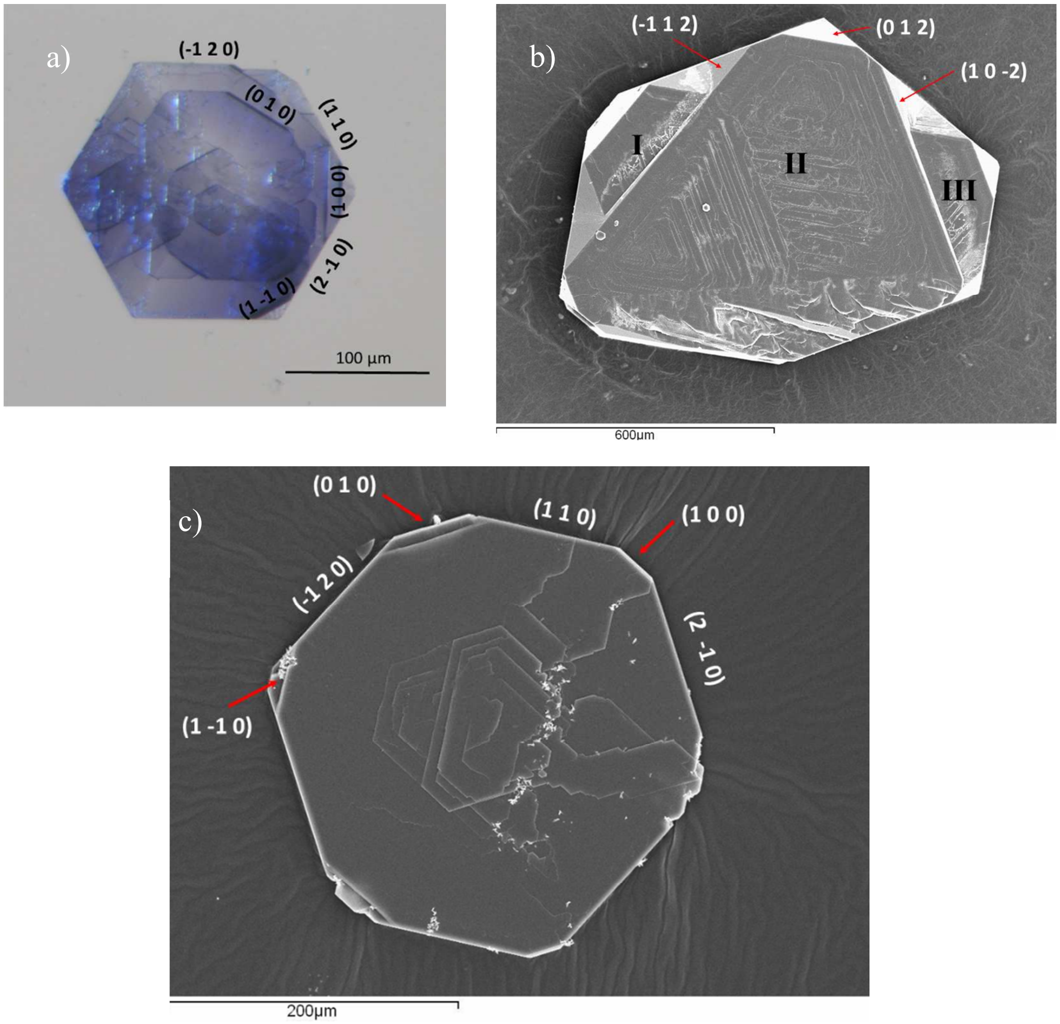

Figure 8. a) An optical picture of a dodecagonal prism crystal of **1** with the Miller indices of the faces. b) SEM image of a twinned crystal of **1** with three main components (I to III) in a perfect hexagonal alignment. c) SEM image of a hexagonal plate of **1** with the Miller indices of the faces. In the core, the growth

lines of a screw dislocation can be seen.

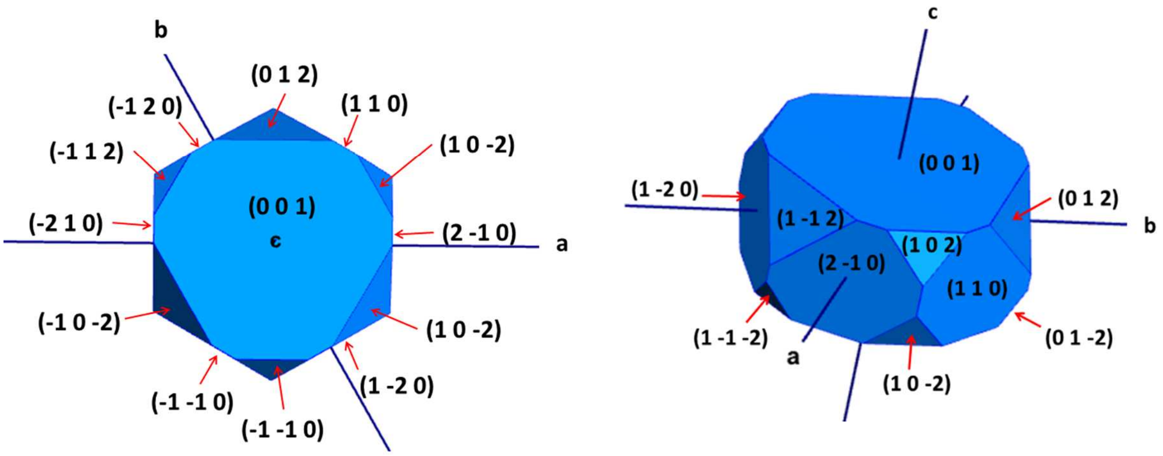

Figura 9. Representation of the crystal morphology with faces and axes numbering (WinXMorph software).[50]

At early stages of the growth, the primary crystal shape is found to be a triangle with truncated vertices (Figure 10). From there, there is one edge growing faster than the others, which occur when the dominant growth mechanism is spiral growth and volume diffusion is the main transport mechanism (Figure 8 and S10).[51,52] Two different sources for the screw dislocations can be appointed, the merging nanocrystallites growing on a flat surface[53] and stacking faults on the (001) face of the cubic close packed structure. In our crystal growth experiments, pure spiral growth has never been achieved, and it is always coexistent with 2D nucleation. An AFM mapping of the surface of a (001) face reveals steps of 0.8 nm height, which is not an unit cell dimension but the thickness of a single layer of $\{[Cu(pmta)]_3cyam\}^{3+}$ molecules (Figure S11 y S12). Therefore, it seems that the hexagonal plate morphology of the crystals is related to the layered distribution of the $\{[Cu(pmta)]_3cyam\}^{3+}$ cations, and the growth along the *c* axis by alternation of perchlorate anions and cations is less favored. Due to the cubic close packing disposition of the cations in the *ABCABC* sequence, the formation of a new layer after the perchlorate one is prone to start a different sequence, and thus, a new crystallite in a different orientation.

Several thin crystals appear on top of each other (Figure 10) with their relative orientation constant as in an oriented aggregation mechanism.[54] We performed a search of the different crystal orientations measuring several crystals at the single crystal X-ray diffractometer, and all the UB matrices of the twin components fitted from the diffraction pattern exhibit rotations of 60, 120 or 180 degrees along the [001] axis respect to the main component.

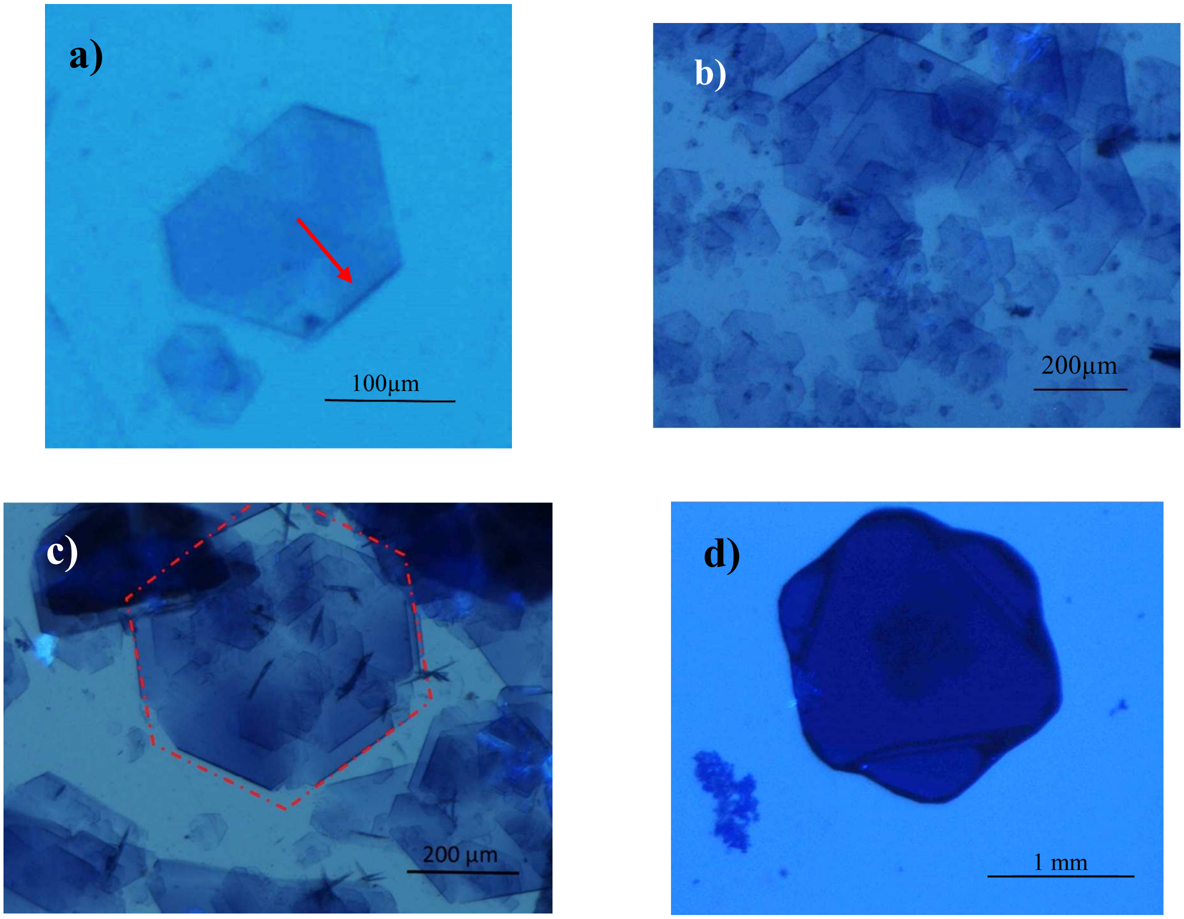

Figure 10. a) Truncated triangular crystal, the arrow show the preferred direction of growth, b) and c) oriented alignment of crystals with low density at the center, the dashed red line in (c) is

an eye guide of the hexagonal morphology of the crystal cluster. d) hexagonal prism of **1**.

The resulting crystals exhibit a fine shape on the edges of the hexagonal prims and a depression in the center (Figure S13), this concavity formed by small crystals induces the dissolution of the crystal core and the growth of the sidewalls by an Ostwald ripening process to finally get the hollow crystals (Figure 6). This process of oriented attachment, and perfection of the crystal via Ostwald ripening has been previously stated for hollow structures.[18,19,26-28,55] These hollow structures are microtubular,[18-20,26-28] octahedral,[23] cubes[56] or even spheres in the form of mesocrystals[57] but hollow plates as that of **1** have only found during the crystallization of ice.[58] Moreover, the size of these hollow structures range from the nanometer scale to a few microns, but the hollow hexagonal prisms of **1** have sizes of *ca*. 300 μm with a hollow of *ca*. 250 μm in diameter (Figure 6). Hollow crystals of these dimensions or even larger have been reported for systems growth by vapor deposition,[52] but it is far less common in solution.[26,27,59]

These astonishing hollow structures that challenge logical comprehension of the nature crystal growth may have a direct impact on the properties and applications they can exhibit. And, they certainly have risen a growing interest in the synthesis and design of this hollow crystals.[23]

4. Conclusions

Based on previous computational knowledge about the cyamelurate molecule as good anion binding group, we have designed and synthetized a copper(II) cyamelurate complex. The coordination positions of the Cu(II) were adequately blocked with a coligand to form a trinuclear C_3 symmetric complex, which crystallizes in the non-centrosymmetric $R3c$ space group and exhibit a cubic close packed arrangement of the molecules. In the solid state, it shows anion-π interactions between the heptazine core and two perchlorate anions above and below the planar group. We have carried out DFT calculations to evaluate the binding energy of this interaction, being *ca*. 175 kcal/mol for the perchlorate:**1** adduct and *ca*. 297 kcal/mol for the ternary complex. Various systems were modeled and the binding energies computed to hierarchize the different contributions leading to electrostactic effects were mainly responsible for the interaction observed in **1**. Contributions from the H-bonding and the pure anion-π interaction were not negligible, but comparable to other systems. Dielectric properties were measured for **1** and a semiconductor behaviour was observed with increased conductivity with the temperature, mainly due to reorganization of the perchlorate anions. The magnetic properties show very weak antiferromagnetic interactions between the copper(II) ions within the trinuclear complex as expected for an electron deficient group as magnetic exchange pathway. The crystals of **1** grow in the form of truncated hexagonal prisms, which exhibit a depression in the center. In some cases, the tiny crystals that form the core, following a process of dissolution and recrystallization, yield completely hollow structures.

ASSOCIATED CONTENT

The Supporting Information contents the synthesis of the cyamelurate ligand, some selected crystal structure parameters together with additional figures of the crystal packing and a detailed description of the dielectric measurements and the magnetic properties. Also, the SI includes SEM, AFM and optical images of the crystals of **1**.

CCDC 977070 contains the supplementary crystallographic data for this paper. These data can be obtained free of charge via www.ccdc.cam.ac.uk/data_request/cif, or by email- ing data_request@ccdc.cam.ac.uk, or by contacting The Cambridge Crystallographic Data Centre, 12 Union Road, ■Cambridge CB2 1EZ, UK; fax: +44 1223 336033.

ACKNOWLEDGEMENTS

Financial support from MINECO (Spain) through the projects MAT2014-57465-R and CTQ2014-57393-C2-1-P (FEDER funds) and from the FONDECYT Project Nº1150747 (Chile) is gratefully acknowledged. C.M.B. thanks the Agencia Canaria de Investigación, Innovación y Sociedad de La información (ACIISI) for a PhD fellowship co-funded by the ESF. ESRF synchrotron and A. Labrador are acknowledged for the HS3902 project that provide the beamtime at BM16. We thank the SEGAI services of the University of La Laguna for the access to the equipment and especially to A. Hernández-Creus for the AFM measurements.

REFERENCES

(1) Busschaert, N.; Caltagirone, C.; Van Rossom, C.; Gale, P. A. Applications of Supramolecular Anion Recognition. *Chem. Rev.* **2015**, *115*, 8038-8155.

(2) Evans, N. H.; Beer, P. D. Advances in Anion Supramolecular Chemistry: From Recognition to Chemical Applications, *Angew. Chem. Int. Ed.* **2014**, *53*, 11716-11754.

(3) Estarellas, C.; Frontera, A.; Quiñonero, D.; Deyà, P. M. Relevant anion-π interactions in biological systems: The case of urate oxidase, *Angew. Chem. Int. Ed.* **2011**, *50*, 415-418.

(4) Bauzá, A.; Mooibroek, T. J.; Frontera, A. The Bright Future of Unconventional σ/π-Hole Interactions. *Chem. Phys. Chem.* **2015**, *16*, 2496-2517.

(5) Frontera, A.; Gamez, P.; Mascal, M.; Mooibroek, T. J.; Reedjik, J. Putting Anion-π into Perspective. *Angew. Chem. Int. Ed.* **2011**, *50*, 9564-9583.

(6) Molina, P.; Zapata, F.; Caballero, A. Anion Recognition Strategies Based on Combined Noncovalent Interactions. *Chem. Rev.* **2017**, *117*, 9907-9972.

(7) Giese, M.; Albrecht, M.; Rissanen, K. Experimental investigation of anion-pi interactions – applications and biochemical relevance, *Chem. Commun.* **2016**, *52*, 1778-1795.

(8) Frontera, A.; Quiñonero D.; Deyà, P. M. Cation-π and anion-π interactions. *WIREs Comput. Mol. Sci.* **2011**, *1*, 440–459.

(9) Kim, D. Y.; Singh, N. J.; Kim, K. S. Cyameluric Acid as Anion-π Type Receptor for ClO_4^- and NO_3^-: π-Stacked and Edge-to-Face Structures. *J. Chem. Theory Comput*. **2008**, *4*, 1401-1407.

(10) Frontera, A. Encapsulation of anions: Macrocyclic receptors based on metal coordination and anion-π interactions. *Coord. Chem. Rev*. **2013**, 257, 1716.

(11) Demeshko, S.; Dechert, S.; Meyer, F. Anion-π interactions in a carousel copper(II)-triazine complex, *J. Am. Chem. Soc.* **2004**, *126*, 4508-4509.

(12) Sattler, A.; Budde, M. R.; Schnick, W. Metal(II) Cyamelurates Prepared from Aqueous Ammonia. *Z. Anorg. Allg. Chem.* **2009**, *635*, 1933–939.

(13) El-Gamel, N. E. A.; Seyfarth, L.; Wagler, J.; Ehrenberg, H.; Schwarz, M.; Senker, J.; Kroke, E. The Tautomeric Forms of Cyameluric Acid Derivatives. *Chem. Eur. J.* **2007**, *13*, 1158–1173.

(14) Horvath-Bordon, E.; Kroke, E.; Svodoba, I.; Fueß, H.; Riedel, R.; Neeraj, S.; Cheetham, A. K. Alkalicyamelurates, $M_3[C_6N_7O_3]\cdot xH_2O$, M = Li, Na, K, Rb, Cs: UV-luminescent and thermally very stable ionic tri-s-triazine derivatives. *Dalton Trans.* **2004**, 3900-3908.

(15) Braml, N. E.; Schnick, W. New Heptazine Based Materials with a Divalent Cation – $Sr[H_2C_6N_7O_3]_2\cdot 4H_2O$ and $Sr[HC_6N_7(NCN)_3]\cdot 7H_2O$, *Z. Anorg. Allg. Chem.* **2013**, *639*, 275-279.

(16) Purdy, A. P.; Case, S.; George, C. Ammonothermal crystal growth of germanium and its alloys: Synthesis of a hollow metallic crystal. *Cryst. Growth Des.* **2003**, *3*, 121-124.

(17) Morin, S. A.; Bierman, B. M.; Tong, J.; Jin, S. Mechanism and kinetics of spontaneous nanotube growth driven by screw dislocations, *Science* **2010**, *5977*, 476-480.

(18) López-Periago, A.; Vallcorba, O.; Domingo, C.; Ayllón, J. A. Hollow microcrystals of copper hexafluoroacetylacetonate-pyridine derivative adducts via supercritical CO_2 recrystallization. *Cryst. Growth Des.* **2016**, *16*, 1725-1736.

(19) Hatano, E.; Morimoto, M.; Imai, T.; Hyodo, K.; Fujimoto, A.; Nishimura, R.; Sekine, A.; Yasuda, N.; Yokojima, S.; Nakamura, S.; Uchida, K. Photosalient Phenomena that Mimic *Impatiens* are Observed in Hollow Crystals of Diarylethene with a Perfluorocyclohexene Ring. *Angew. Chem. Int. Ed.* **2017**, *56*, 12576-12580.

(20) Martins, D.; Stelzer, T.; Ulrich, J.; Coquerel, G. Formation of Crystalline Hollow Whiskers as Relics of Organic Dissipative Structures, *Cryst. Growth Des.* **2011**, *11*, 3020-3026.

(21) Bhargavi, N.; Chavan, R. B.; Shastri, N. R. Generation of Hollow Crystals of a drug with Lamellar Structure Forming Ability, *Cryst. Growth Des.* **2017**, *17*, 1480-1483.

(22) Bhargavi, N.; Chavan, R. B.; Shastri, N. R. Hollow Crystal generation through polymorphic transformation – a case study of flufenamic acid, *CrystEngComm* **2018**, *20*, 275-279.

(23) Wang, X.; Yu, L.; Hu, P.; Yuan, F. Synthesis of Single Crystalline Hollow Octahedral NiO. *Cryst. Growth Des.* **2007**, *7*, 2415-2418.

(24) Wang, H.; Xin, L.; Wang, H.; Yu, X.; Liu, Y.; Zhou, X.; Li, B. Aggregation-induced growth of hexagonal ZnO hierarchical mesocrystals with interior space: nonaqueous synthesis, growth mechanism, and optical properties. *RSC Advances.* **2013**, *3*, 6538.

(25) Chen, X.; Qiao, M.; Xie, S.; Fan, K.; Zhou, W.; He, H. Self-construction of core-shell and hollow zeolite analcime icositetrahedra: a reversed crystal growth process via oriented aggregation of nanocrystallites and recrystallization from surface to core, *J. Am. Chem. Soc.* **2007**, *129*, 13305-13312.

(26) Pérez-Hernández, N.; Fort, D.; Pérez, C.; Martín, J. D. Water-induced molecular self-assembly of hollow tubular crystals, *Cryst. Growth Des.* **2011**, *11*, 1054-1061.

(27) Castillo-Blas, C.; de la Peña-O'Shea, V. A.; Puente-Orench, I.; Romero de Paz, J.; Sáez-Puche, R.; Gutiérrez-Puebla, E.; Gándara, F.; Monge, A. Addressed realization of multication complex arrangements in metal-organic frameworks, *Sci. Adv.* **2017**, *3*, e1700773.

(28) Zeng, H. C. Ostwald Ripening: A Synthetic Approach for Hollow Nanomaterials. *Curr. Nanosci.* **2007**, *3*, 177-181.

(29) Guzman-Afonso, C; Gonzalez-Silgo, C; Torres, M.E. ; Matesanz, E.; Mujica, A. Structural anomalies related to changes in the conduction mechanisms of α-$Sm_2(MoO_4)_3$. *J. Phys.: Condens. Matter*, **2013**, *25(3)*, 035902.

(30) Agilent Technologies, "Basics of Measuring the Dielectric Properties of Materials". *Agilent application note*. **2005**, 5989-2589EN, April 28.

(31) Ahlrichs, R.; Bär, M.; Hacer, M.; Horn, H.; Kömel, C. Electronic structure calculations on workstation computers: The program system turbomole. *Chem. Phys. Lett*. **1989**, *162*, 165–169.

(32) Gerenkamp, M.; Grimme, S. Spin-component scaled second-order Møller–Plesset perturbation theory for the calculation of molecular geometries and harmonic vibrational frequencies. *Chem. Phys. Lett*. **2004**, *392*, 229-235.

(33) Boys, S. B.; F. Bernardy, S. B. The calculation of small molecular interactions by the differences of separate total energies. Some procedures with reduced errors. *Mol. Phys*., **1970**, *19*, 553–566.

(34) Otwinowski, Z.; Minor, W.; Carter, C. W. Jr.; Sweet, R. M. Eds. Academic Press, New York, 1997, In *Methods in Enzymology*, Vol. 276: *Macromolecular Crystallography*, part A, 307–326.

(35) Sheldrick, G. M. A short history of *SHELX. Acta Cryst*. **2008**, *A64*, 112–122.

(36) Farrugia, J. L. *WinGX* suite for small-molecule single-crystal crystallography. *J. Appl. Cryst.* **1999**, *32*, 837.

(37) Spek, A. L. Single-crystal structure validation with the program *PLATON. J. Appl. Cryst.,* **2003**, *36*, 7-13.

(38) DIAMOND 4.4.1, Crystal Impact GbR, CRYSTAL IMPACT, K. Brandenburg& H. Putz GbR, Postfach1251, D-53002 Bonn, Germany, 2000.

(39) Yang, L.; Powell. D. R.; Houser, R. P. Structural variation in copper(I) complexes with pyridylmethylamide ligands: structural analysis with a new four-coordinate geometry index, τ_4. *Dalton Trans.* **2007**, 955-964.

(40) Brewer, G,; Butcher, R. J.; Lear, S.; Noll, B.; Zavalij, P. Y. Synthesis, structure and supramolecular features of cobalt(III) and cobalt(II) complexes, $[CoH_xL](ClO_4)_y$ (x = y = 3, 2,

1.50, 1.45, 1 and 0 and x = 3, y = 2) of a triprotic imidazole containing Schiff base ligand. Effect of protonation state on supramolecular structure. *Inorg. Chim. Acta*, **2014**, *410*, 94-105.

(41) Farrar, J. A.; McKee, V.; Al-Obaidi, A. H. R.; McGarvey, J. J.; Nelson, J., Thomson, A.J. Spectroscopic Studies on the Average-Valence Copper Site $[Cu_2]^{3+}$. *Inorg. Chem.* **1995**, *34*, 1302-1303.

(42) Gamez, P. The anion–π interaction: naissance and establishment of a peculiar supramolecular bond. *Inorg. Chem. Front.* **2014**, *1*, 35-43.

(43) Braga, D.; Grepioni, F.; Desiraju, G. R. Crystal Engineering and Organometallic Architecture. *Chem. Rev.* **1998**, *98*, 1375-1405.

(44) Chifotides, H. T.; Dunbar, K. R. Anion−π Interactions in Supramolecular Architectures. *Acc. Chem. Res.* **2013**, *46*, 894–906.

(45) Domasevitch, K. V.; Solntsev, P. V.; Gural'skiy, I. A.; Krautscheid, H.; Rusanov, E. B.; Chernega, A. N.; Howard, J. A. K. Silver(I) ions bridged by pyridazine: doubling the ligand functionality for the design of unusual 3D coordination frameworks. *Dalton Trans*. **2007**, *35*, 3893–3905.

(46) Jonscher, A.K. *Dielectric Relaxation in Solids*, Chelsea Dielectric Press, London, 1983.

(47) Lee, W. K.; Liu, J. F.; Nowick. A. S. Limiting behavior of ac conductivity in ionically conducting crystals and glasses: A new universality. *Phys. Rev. Lett*. **1991**, *67*, 1559.

(48) Pradhan, D. K.; Behera, B.; Das. P. R. Studies of dielectric and electrical properties of a new type of complex tungsten bronze electroceramics. *J. Mater. Sci.: Mater. Electron.* **2012**, *23(3)*, 779-785.

(49) Almond, D. P.; Duncan, G. K.; West, A. R. The determination of hopping rates and carrier concentrations in ionic conductors by a new analysis of ac conductivity, *Solid State Ionics*, **1983**, *8(2)*, 159-164.

(50) Kaminsky, W. From CIF to virtual morphology using the WinXMorph program, *J. Appl. Cryst.* **2007**, *40*, 382-385.

(51) Sangwal, K. Growth kinetics and surface morphology of crystals grown from solutions: Recent observations and their interpretations. *Prog. Crystal Growth and Charact.* **1998**, *36*, 163-248.

(52) Simov, S. Morphology of hollow crystals of II-VI compounds, *J. Mater. Sci.* **1976**, *11*, 2319-2332.

(53) Thürmer, K.; Bartelt, N. C. Growth of multilayer ice films and the formation of cubic ice imaged with STM. *Phys. Rev. B* **2008**, *77(19)*, 195425.

(54) Wang, F.; Wang, X. Mechanisms in the solution growth of free-standing two-dimensional inorganic nanomaterials. *Nanoscale*, **2014**, *6*, 6398-6414.

(55) García-Tuñón, E.; Couceiro, R.; Franco, J.; Saiz, E.; Guitián, F. Synthesis and characterisation of large chlorapatite single-crystals with controlled morphology and surface roughness. *J. Mater. Sci.: Mater. Med.* **2012**, *23*, 2471-2482.

(56) Dai, C.; Zhang, A.; Li, L.; Hou, K.; Ding, F.; Li, J.; Mu, D.; Song, C.; Liu, M.; Guo, X. Synthesis of Hollow Nanocubes and Macroporous Monoliths of Silicalite-1 by Alkaline Treatment. *Chem. Mater.* **2013**, *25*, 4197-4205.

(57) Wang, D.; Du, S.; Zhou, X,; Wang, B.; Ma, J.; Sun, P.; Sun, Y.; Lu, G. Template-free synthesis and gas sensing properties of hierarchical hollow ZnO microspheres, *CrystEngComm* **2013**. *15*, 7438-7442.

(58) Smith, H. R.; Connolly, P. J.; Baran, A. J.; Hesse, E.; Smedlet, A. R. D.; Webb, A. R. Cloud chamber laboratory investigations into scattering properties of hollow ice particles. *J. Quant. Spectrosc. Radiat. Transf.* **2013**, *129*, 169-185.

(59) Perry, A. R.; Peruffo, M.; Unwin, P.R. Quantitative Plane-Resolved Crystal Growth and Dissolution Kinetics by Coupling In Situ Optical Microscopy and Diffusion Models: The Case of Salicylic Acid in Aqueous Solution, *Cryst. Growth Des.* **2013**, *13*, 614-622.

For table of contents use only

Anion-π interactions in hollow crystals of a copper(II)-cyamelurate coordination complex

Carla Martínez-Benito,[a] Antonio Bauzá,[b] Ana B. Lago,[a] Catalina Ruiz-Pérez,[a] Claudio A. Jiménez,[c] Manuel E. Torres,[d] Antonio Frontera,[b] and Jorge Pasán*[a]

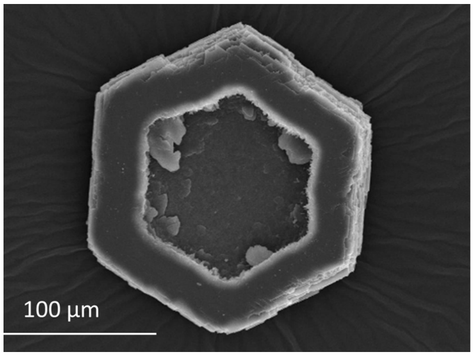

Large hexagonal hollow crystals of a novel cyamelurate-based copper(II) coordination compound designed from a computational approach to show anion-π interactions were prepared. The different contributions to the anion-π interaction were analyzed theoretically and the dielectric and magnetic properties studied. The hollowed crystal morphology has been studied in detail.